First-Principles Calculation of the Bulk Photovoltaic Effect in Bismuth Ferrite

Steve M. Young, Fan Zheng, and Andrew M. Rappe
The Makineni Theoretical Laboratories, Department of Chemistry, University of Pennsylvania, Philadelphia, Pennsylvania 19104-6323, USA
(Received 23 August 2012; published 4 December 2012)

We compute the bulk photovoltaic effect (BPVE) in $BiFeO_3$ using first-principles shift current theory, finding good agreement with experimental results. Furthermore, we reconcile apparently contradictory observations: by examining the contributions of all photovoltaic response tensor components and accounting for the geometry and ferroelectric domain structure of the experimental system, we explain the apparent lack of BPVE response in striped polydomain samples that is at odds with the significant response observed in monodomain samples. We reveal that the domain-wall-driven response in striped polydomain samples is partially mitigated by the BPVE, suggesting that enhanced efficiency could be obtained in materials with cooperative rather than antagonistic interaction between the two mechanisms.

DOI: 10.1103/PhysRevLett.109.236601 PACS numbers: 72.40.+w, 73.50.Pz, 77.84.−s, 78.20.Bh

Ferroelectrics have recently received a great deal of interest as photovoltaic materials [1–7]. Unlike traditional photovoltaic devices, ferroelectrics do not require *p-n* junctions to generate photocurrents. In fact, ferroelectrics do not necessarily need separation of electrons and holes by internal fields at all; photocurrent and photovoltage can be observed in pure homogeneous single crystals. This is known as the bulk photovoltaic effect [8–11]. As a result, ferroelectric oxide materials including $LiNbO_3$ and $BaTiO_3$ have been widely studied for their photovoltaic properties, with substantial effort devoted to understanding their origins [5–7,9,12–20].

$BiFeO_3$ (BFO) is a well-known multiferroic material that displays both large (90 $\mu C/cm^2$) polarization and weak ferromagnetism [21]. Furthermore, it possesses a relatively small band gap (2.74 eV) that falls in the visible spectrum [22]. This presents a major advantage over other ferroelectric oxides with large band gaps (typically $\approx$3.5 eV). There has been a flurry of interest in $BiFeO_3$ as a photovoltaic, highlighting it as a viable candidate for ferroelectric-based photovoltaic devices [1–4,7].

However, the origin of the observed photovoltaic properties is not quite clear. Recently, large photovoltages have been observed opposite the direction of material polarization in BFO [3,4]. The photovoltage was attributed to the periodic domain walls acting to both separate and collect photoexcited carriers. The strong dependence of photovoltage on the density of domain walls supports this hypothesis. However, while the bulk photovoltaic effect, as observed in crystals such as $LiNbO_3$, was discarded as a primary mechanism for the large photovoltages, the existence and impact of such an effect could not be ruled out or quantified. Indeed, other studies of BFO evaluated the photovoltaic responses parallel [7] and perpendicular [1] to the ferroelectric polarization direction and observed substantial photocurrent generation, strongly suggesting that this effect should be significant even in samples with domain walls. The photocurrent in BFO has also been reported as being generated uniformly throughout the sample, consistent with a bulk effect [23]. Understanding the contributions of various mechanisms involved in the response collinear with material polarization is difficult, as the experiments cannot separate the bulk photovoltaic effect from polarization-dependent mechanisms like those in Refs. [3,4]. Previously, we have demonstrated the ability to compute the bulk photovoltaic response tensor in oxides from first principles [24]. In the present Letter, we calculate the shift current response for BFO, showing good agreement with the results from Ref. [1] and providing estimates of the photocurrents collinear with the material polarization. Using these results, we are able to determine the impact of the bulk photovoltaic effect on the system studied in Refs. [3,4], explaining its apparent absence.

In Ref. [24], it was demonstrated that the so-called "shift current" is the dominant mechanism of the bulk photovoltaic effect in ferroelectric oxides $BaTiO_3$ and $PbTiO_3$. As shown there, and also in Refs. [13,25], a perturbative treatment with a classical electromagnetic field in the dipole approximation yields the expression

$$\begin{aligned} J_q &= \sigma_{rsq} E_r E_s \\ \sigma_{rsq}(\omega) &= \pi e \left(\frac{e}{m\hbar\omega}\right)^2 \sum_{n',n''} \int d\mathbf{k} (f[n''\mathbf{k}] - f[n'\mathbf{k}]) \\ &\quad \times \langle n'\mathbf{k}|\hat{P}_r|n''\mathbf{k}\rangle\langle n''\mathbf{k}|\hat{P}_s|n'\mathbf{k}\rangle \\ &\quad \times \left(-\frac{\partial \phi_{n'n''}(\mathbf{k},\mathbf{k})}{\partial k_q} - [\chi_{n''q}(\mathbf{k}) - \chi_{n'q}(\mathbf{k})]\right) \\ &\quad \times \delta(\omega_{n''}(\mathbf{k}) - \omega_{n'}(\mathbf{k}) \pm \omega) \end{aligned} \quad (1)$$

where n' and n'' index the bands, $\mathbf{k}$ is the wave vector, $\omega_n(\mathbf{k})$ is the energy of the nth band, and σ_{rsq} is a third-rank tensor giving current density $\mathbf{J}$ as a response to electromagnetic field $\mathbf{E}$.

The expression is composed of a transition intensity multiplied by the so-called shift vector

$$R_q(n', n'', \mathbf{k}) = -\frac{\partial \phi_{n'n''}(\mathbf{k}, \mathbf{k})}{\partial k_q} - [\chi_{n''q}(\mathbf{k}) - \chi_{n'q}(\mathbf{k})], \tag{2}$$

where χ_n are the Berry connections for band n and $\phi_{nn'}$ is the phase of the momentum matrix element between bands n and n'. The shift vector describes, on average, the displacement of coherent carriers during their lifetimes.

The Glass coefficient [10]

$$G_{rrq} = \frac{\sigma_{rrq}(\omega)}{\alpha_{rr}(\omega)} \tag{3}$$

describes the current response in a thick sample and includes the effect of light attenuation due to absorption coefficient $\alpha_{rr}(\omega)$.

BFO belongs to space group $R3c$. Shown in Fig. 1 is the primitive (10 atom) unit cell with the polarization direction along [0001] (z direction), as well as the relation to the pseudocubic unit cell sometimes used, for which the polarization is along the [111] direction. BFO is nearly a G-type antiferromagnetic material; however, it is found that there is spin canting in the xy plane (perpendicular to the polarization direction) [26]. Because of the small magnitude ($\approx 0.1\ \mu$B per unit cell), this spin canting is ignored in the present Letter and only spin-polarized calculations are performed. The experimental geometry is used for calculations throughout.

In the coordinates of this geometry, a third-rank tensor, such as the shift current response tensor, must have the form

$$\sigma = \begin{bmatrix} 0 & 0 & 0 & 0 & \sigma_{yzY} & -\sigma_{yyY} \\ -\sigma_{yyY} & \sigma_{yyY} & 0 & \sigma_{yzY} & 0 & 0 \\ \sigma_{xxZ} & \sigma_{xxZ} & \sigma_{zzZ} & 0 & 0 & 0 \end{bmatrix}, \tag{4}$$

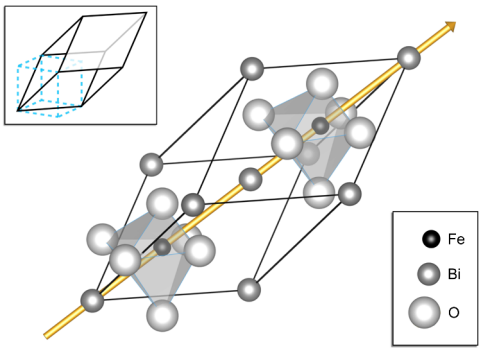

FIG. 1 (color online). The rhombohedral unit cell of bismuth ferrite with the polarization direction denoted by the gold arrow. The two iron atoms are coordinated by distorted octahedral oxygen cages, rotated in opposite directions. The structure is only slightly distorted from the cubic perovskite structure, so the pseudocubic unit cell, shown in the inset in relation to the rhombohedral unit cell, is often used to represent the structure.

where the electric field degrees of freedom have been condensed to a single dimension, as in Voigt notation. For clarity, we show the tensor index corresponding to current direction in upper case letters, while the indices giving the light polarization are in lower case letters. We note that the above tensor is Cartesian, such that the rhombohedral lattice vectors in terms of Cartesian coordinates are, by convention, $\vec{A}_1 = (\frac{a}{2}, -\frac{a}{2\sqrt{3}}, \frac{c}{3})$, $\vec{A}_2 = (0, \frac{a}{\sqrt{3}}, \frac{c}{3})$, $\vec{A}_3 = (-\frac{a}{2}, -\frac{a}{2\sqrt{3}}, \frac{c}{3})$.

The QUANTUM-ESPRESSO plane-wave density functional theory (DFT) package was used to perform the DFT calculation with a generalized gradient approximation functional [27]. Norm-conserving, designed nonlocal pseudopotentials were generated with the OPIUM package [28,29]. All pseudopotentials, including iron [30], were found to converge within a plane-wave cutoff energy of 50 Ry. We note that the inclusion of semicore states in iron was crucial for obtaining the correct behavior. The self-consistent calculation was first performed on an $8 \times 8 \times 8$ k-point grid in order to produce the input charge density. Next, non-self-consistent calculations were performed on denser grids as needed to converge the results. Due to the well-known tendency of DFT calculations to underestimate the localization of the d-orbital electrons, the DFT + U method is used in the calculation, including an effective Hubbard $U_{\text{eff}} = U\text{-}J$ in the Hamiltonian. In order to choose the proper U_{eff} value, the imaginary permittivity was calculated in the long wavelength approximation with different U_{eff} values and compared to experiment. Shown in Fig. 2(a) are the real and imaginary permittivities, with experimental data taken from Ref. [22]. We find that the calculation with GGA + $U_{\text{eff}} = 5$ eV best matches the experimental imaginary permittivity (dielectric loss) for energies near the band gap, especially the energies of the t_{2g} and e_g peaks. As is commonly the case with DFT calculations, due in part to the absence of quasiparticle corrections [31], the magnitude of the permittivity is substantially overestimated. This can been observed in hematite, as well [32,33], which is structurally and chemically similar to BFO. For additional calibration, we calculate the

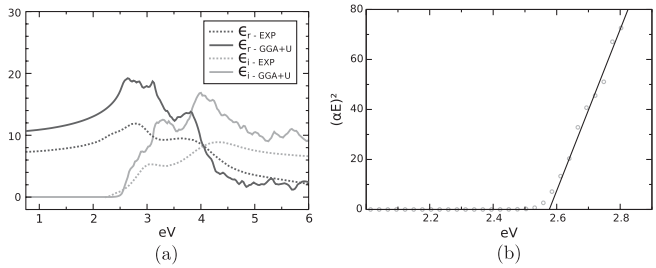

FIG. 2. In (a), the calculated components of the permittivity, ϵ, are compared to experiment. In (b), the calculated band gap is shown to be 2.58 eV, 0.16 eV less than the experimentally determined value of 2.74 eV [22].

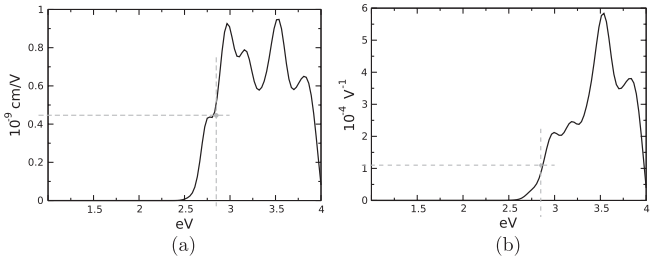

FIG. 3. (a) The calculated Glass coefficient, G_{yyY}, and (b) bulk photovoltaic coefficient, σ_{yyY}, are shown, with the experimental values marked for comparison [1].

gap using the same method in Ref. [22], shown in Fig. 2(b), and find that the calculated value underestimates the experimental gap by 0.16 eV.

Shown in Fig. 3 are the calculated photovoltaic tensor elements and Glass coefficients that yield current in the Y direction in the plane normal to the polarization axis, compared with the experimental results from Ref. [1].

We have adjusted our results to account for the slightly lower band gap, shifting them right by 0.16 eV. Compared to the experimental measurements of Glass coefficient and shift current tensor ($G_{yyY} = 4.48 \times 10^{-10}$ cm/V and $\sigma_{yyY} = 1.1 \times 10^{-4}$ V^{-1} around the photon energy of 2.85 eV in Ref. [1]), our results agree very well.

The complete shift current and Glass coefficient tensors can be found in the Supplemental Material [34].

In Ref. [3], the photovoltaic response to unpolarized light is measured in a thin film with parallel 71° domain walls. The orientation of domains in the experimental setup is shown in Fig. 4. The net material polarization is normal to the domain walls, and the photocurrent is measured both parallel and perpendicular to the in-plane component of net material polarization, while photovoltage is measured only parallel to the in-plane component of net material

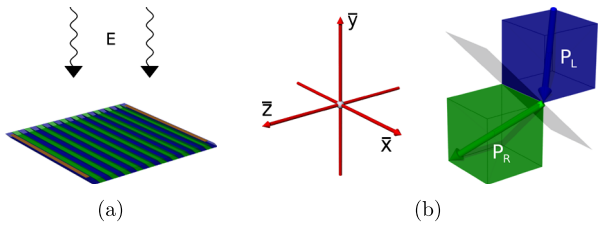

FIG. 4 (color online). The experimental setup of Refs. [3,4]. The film shown in (a) is composed of alternating domains with polarizations of adjacent domains at 71° angles to one another. Large photovoltages and photocurrents are observed when electrodes, appearing as strips on top of the terminal domains, are placed parallel to the domains. No response is observed when the electrodes are perpendicular to the domains (not shown). In (b), the orientation of the pseudocubic unit cell and polarization for each domain are shown, along with the principal axes of the experimental coordinate frame. The domains are labeled one with the letter R and the color green, and the other with the letter L and the color blue.

polarization. While high response in the antiparallel direction is observed for polydomain samples, with photovoltage scaling linearly with domain density, little or no photovoltage is detected for monodomain crystals, and negligible photocurrent is measured perpendicular to net polarization, supporting the proposed mechanism of domain-wall-driven generation of large photovoltages. However, based on the results for photocurrent in the plane normal to the polarization obtained in Ref. [1], the authors speculate that the bulk photovoltaic response along the polarization direction should be significant. This view is supported by their studies of the photocurrent parallel to polarization [7].

The calculated response tensor elements yielding current in the material polarization direction are shown in Fig. 5. The direction is uniformly parallel, rather than antiparallel, to the material polarization, and similar in magnitude to the in-plane response. These results appear to confirm that the bulk photovoltaic effect constitutes a meaningful contribution to the response observed in the experimental setup. However, the geometry of the system shown in Fig. 4, especially the orientation of the domain polarization to the incident illumination, suggests a more complicated picture, as many different tensor elements will contribute to the observed response. As evident from Eq. (4), some of these elements have opposite sign from one another, allowing for the possibility that significant cancellations may occur. To properly calculate the response, the field of the incoming radiation must first be expressed in the coordinate system of the material, as used to express the response tensor. For both domains,

$$\mathbf{E}(\theta) = E_0 \begin{bmatrix} \cos(\theta) \\ \sin(\theta)\sqrt{\frac{1}{3}} \\ \sin(\theta)\sqrt{\frac{2}{3}} \end{bmatrix} \tag{5}$$

for light with wave vector parallel to $\bar{y}$ and polarization angle θ to x_L/x_R. In accordance with Malus's law,

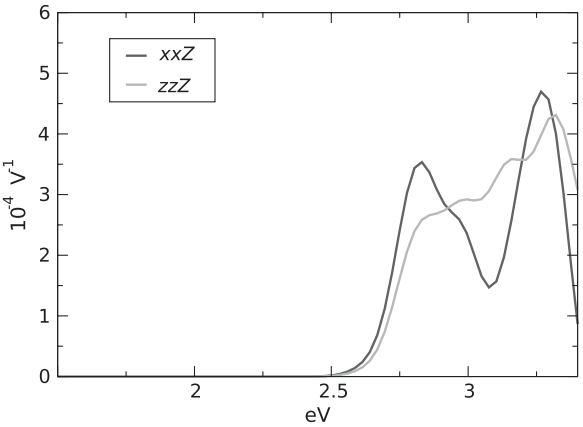

FIG. 5. The photovoltaic response tensor elements for current collinear with the material polarization.

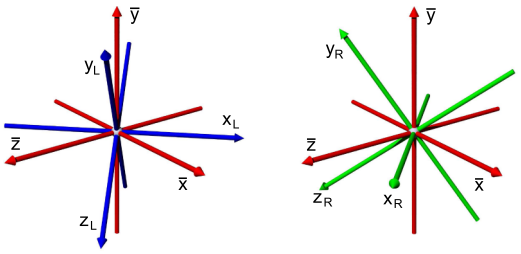

FIG. 6 (color online). The relationship between the principal axes of the material coordinates and the lab coordinates ($\bar{x}$, $\bar{y}$, $\bar{z}$) in Fig. 4. The z_R and z_L axes are parallel to the polarization in their respective domains; the x_R and x_L are in the $\bar{x}\,\bar{z}$ plane; and y_R and y_L complete the orthogonal bases.

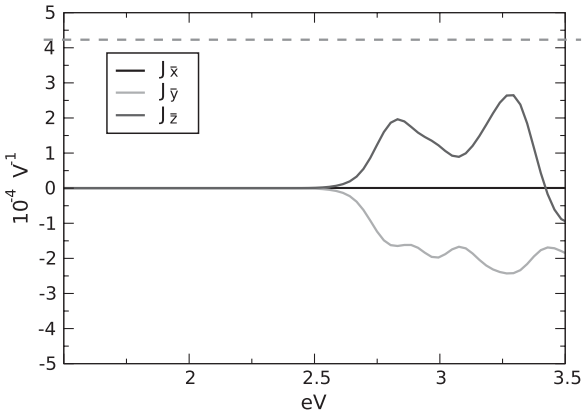

FIG. 7. The calculated current densities per light intensity in the lab frame of the BFO film, with the experimental value from Ref. [3] marked by the dashed red line. The current in the $\bar{x}$ direction, parallel to the domain walls, vanishes, while much of the remaining current is directed toward the bottom of the sample.

unpolarized light can be decomposed into any two fields of perpendicular polarization; we select θ to be 0° and 90° for both domains. After computing the response in the material frame, we must rotate the current density vector back into the lab coordinate system. Thus, for unpolarized, overhead illumination, the total response can be calculated as

$$J_l = R^R_{lk}\left[\sigma_{ijk}\frac{E_i(0°)E_j(0°) + E_i(90°)E_j(90°)}{2}\right] + R^L_{lk}\left[\sigma_{ijk}\frac{E_i(0°)E_j(0°) + E_i(90°)E_j(90°)}{2}\right],$$

where R^R and R^L rotate from the principal axes of the two domain types, denoted as (x_R, y_R, z_R) and (x_L, y_L, z_L) and shown in green and blue, respectively, in Fig. 6, to experimental coordinates, denoted as ($\bar{x}$, $\bar{y}$, $\bar{z}$) and shown in red, where $\bar{z}$ is parallel to the in-plane component of net material polarization, $\bar{y}$ is normal to the film surface, and $\bar{x}$ is orthogonal to $\bar{y}$ and $\bar{z}$, forming a right-handed coordinate system. In the barred system,

$$x_R = \left(\frac{1}{\sqrt{2}}, 0, \frac{1}{\sqrt{2}}\right), \qquad x_L = \left(\frac{1}{\sqrt{2}}, 0, -\frac{1}{\sqrt{2}}\right),$$

$$y_R = \left(-\frac{1}{\sqrt{6}}, \sqrt{\frac{2}{3}}, \frac{1}{\sqrt{6}}\right), \qquad y_L = \left(\frac{1}{\sqrt{6}}, \sqrt{\frac{2}{3}}, \frac{1}{\sqrt{6}}\right),$$

$$z_R = \left(-\frac{1}{\sqrt{3}}, -\frac{1}{\sqrt{3}}, \frac{1}{\sqrt{3}}\right), \qquad z_L = \left(\frac{1}{\sqrt{3}}, -\frac{1}{\sqrt{3}}, \frac{1}{\sqrt{3}}\right).$$

The components of the total current in the lab frame are shown in Fig. 7. The current in the $\bar{x}$ direction—parallel to the domain walls—vanishes, in agreement with experiment. The current in the $\bar{z}$ direction is substantial, however, and proceeds in the opposite direction of the experimental response, indicating that the two photovoltaic effects partially cancel. The magnitude of this component is a large fraction of the experimentally measured current, suggesting that the reduction in current may be significant. In the single-domain case, where the impact of carrier separation at domain walls is suppressed, one might expect a photovoltage in the opposite direction, but experimentally negligible photovoltage was observed. However, a large portion of the current is directed to the lower surface, especially in a thin film geometry. Upon illumination, layers of carriers will form on the surfaces, allowing any charge imbalances between electrodes to rapidly equilibrate without domain-wall traps in between. Thus, any shift current in the $\bar{z}$ direction will be prevented from sustaining a photovoltage in that direction, due to the conductivity of the surfaces resulting from the $\bar{y}$ directed photovoltage. This is also consistent with the observation of significant photocurrent obtained in Ref. [2], where the orientation of the crystal to the incident light is the same but current is measured in the direction perpendicular to that of the setup in Ref. [3].

We have reconciled the large bulk photovoltaic response found in Refs. [1,4] with the apparent negligible contribution evinced in Ref. [3] through first-principles calculations. Importantly, we find that the bulk photovoltaic effect will partially cancel domain-wall-driven carrier separation, indicating that even higher efficiencies may be possible. Effective photovoltaic materials may be found which take advantage of a domain-wall structure of the kind explored in Refs. [3,4], especially as a mechanism of trapping carriers, but relying on the bulk photovoltaic effect to contribute to carrier separation rather than suppress it.

S. M. Y. was supported by the Department of Energy, Office of Basic Energy Sciences, under Grant No. DE-FG02-07ER46431. F. Z. was supported by the Air Force Office of Scientific Research, Air Force Materiel Command, USAF, under Grant No. FA9550-10-1-0248. A. M. R. was supported by the Office of Naval Research under Grant No. N00014-11-1-0578. Computational support was provided by the HPCMO of the DoD.

[1] W. Ji, K. Yao, and Y. C. Liang, Phys. Rev. B **84**, 094115 (2011).
[2] T. Choi, S. Lee, Y. Choi, V. Kiryukhin, and S.-W. Cheong, Science **324**, 63 (2009).
[3] S. Yang, J. Seidel, S. J. Byrnes, P. Schafer, C.-H. Yang, M. Rossel, P. Yu, Y.-H. Chu, J. F. Scott, J. W. Ager, L. Martin, and R. Ramesh, Nat. Nanotechnol. **5**, 143 (2010).
[4] J. Seidel, D. Fu, S.-Y. Yang, E. Alarcón-Lladó, J. Wu, R. Ramesh, and J. W. Ager, Phys. Rev. Lett. **107**, 126805 (2011).
[5] L. Pintilie, V. Stancu, E. Vasile, and I. Pintilie, J. Appl. Phys. **107**, 114111 (2010).
[6] D. W. Cao, H. Zhang, L. A. Fang, W. Dong, F. G. Zheng, and M. R. Shen, Appl. Phys. Lett. **97**, 102104 (2010).
[7] W. Ji, K. Yao, and Y. C. Liang, Adv. Mater. **22**, 1763 (2010).
[8] A. G. Chynoweth, Phys. Rev. **102**, 705 (1956).
[9] F. S. Chen, J. Appl. Phys. **40**, 3389 (1969).
[10] A. M. Glass, D. von der Linde, and T. J. Negran, Appl. Phys. Lett. **25**, 233 (1974).
[11] V. M. Fridkin, Crystallogr. Rep. (Transl. Kristallografiya) **46**, 654 (2001).
[12] W. T. H. Koch, R. Munser, W. Ruppel, and P. Wurfel, Ferroelectrics **13**, 305 (1976).
[13] R. von Baltz and W. Kraut, Phys. Rev. B **23**, 5590 (1981).
[14] B. I. Sturman and V. M. Fridkin, in *The Photovoltaic and Photorefractive Effects in Noncentrosymmetric Materials*, Ferroelectricity and Related Phenomena Vol. 8, edited by G. W. Taylor (Gordon and Breach, New York, 1992).
[15] M. Qin, K. Yao, and Y. C. Liang, Appl. Phys. Lett. **95**, 022912 (2009).
[16] S. R. Basu, L. W. Martin, Y. H. Chu, M. Gajek, R. Ramesh, R. C. Rai, X. Xu, and J. L. Musfeldt, Appl. Phys. Lett. **92**, 091905 (2008).
[17] M. Ichiki, H. Furue, T. Kobayashi, R. Maeda, Y. Morikawa, T. Nakada, and K. Nonaka, Appl. Phys. Lett. **87**, 222903 (2005).
[18] Z. J. Yue, K. Zhao, S. Q. Zhao, Z. Q. Lu, X. M. Li, H. Ni, and A. J. Wang, J. Phys. D **43**, 015104 (2010).
[19] G. L. Yuan and J. L. Wang, Appl. Phys. Lett. **95**, 252904 (2009).
[20] S. Y. Yang, L. W. Martin, S. J. Byrnes, T. E. Conry, S. R. Basu, D. Paran, L. Reichertz, J. Ihlefeld, C. Adamo, A. Melville, Y. H. Chu, C. H. Yang, J. L. Musfeldt, D. G. Schlom, J. W. Ager III, and R. Ramesh, Appl. Phys. Lett. **95**, 062909 (2009).
[21] G. Catalan and J. F. Scott, Adv. Mater. **21**, 2463 (2009).
[22] J. F. Ihlefeld, N. J. Podraza, Z. K. Liu, R. C. Rai, X. Xu, T. Heeg, Y. B. Chen, J. Li, R. W. Collins, J. L. Musfeldt, X. Q. Pan, J. Schubert, R. Ramesh, and D. G. Schlom, Appl. Phys. Lett. **92**, 142908 (2008).
[23] M. Alexe and D. Hesse, Nat. Commun. **2**, 256 (2011).
[24] S. M. Young and A. M. Rappe, Phys. Rev. Lett. **109**, 116601 (2012).
[25] J. E. Sipe and A. I. Shkrebtii, Phys. Rev. B **61**, 5337 (2000).
[26] C. Ederer and N. A. Spaldin, Phys. Rev. B **71**, 060401 (2005).
[27] P. Giannozzi *et al.*, J. Phys. Condens. Matter **21**, 395502 (2009).
[28] A. M. Rappe, K. M. Rabe, E. Kaxiras, and J. D. Joannopoulos, Phys. Rev. B **41**, 1227 (1990).
[29] N. J. Ramer and A. M. Rappe, Phys. Rev. B **59**, 12471 (1999).
[30] T. Sasaki, A. M. Rappe, and S. G. Louie, Phys. Rev. B **52**, 12760 (1995).
[31] S. Lebègue, B. Arnaud, and M. Alouani, Phys. Rev. B **72**, 085103 (2005).
[32] C. T. Chen and B. D. Cahan, J. Opt. Soc. Am. **71**, 932 (1981).
[33] H. Yang, W. Mi, H. Bai, and Y. Cheng RSC Adv. **2**, 10708 (2012).
[34] See Supplemental Material at http://link.aps.org/supplemental/10.1103/PhysRevLett.109.236601 for the complete calculated photovoltaic response tensors.